# Quartz Crystal Microbalance Sensor Based on ZnO–Graphene Thin Film for Gas Detection

M. Boutamine[a,*], Y. Bakha[b], H. Saidani[c],
H. Hachemi[a], A.D. Guerfi[a], C. Sebbah[a],
S. Aberkane[a], H. Khales[b] and A. Bellel[d]

[a]*Research Laboratory in Electronics and Electrical Systems Engineering, Scientific and Technological Research Directorate, Cherchell Academy DPHB, Algeria*
[b]*Electromechanical Microsystems Technology Platform,P-MEMS, Center for Development of Advanced Technologies, August 20, 1956, Baba Hassen, Algiers, Algeria*
[c]*Department of Mechanical Engineering, University of Bristol, EEME School, Queens Building, University Walk, Bristol BS8 1TR, UK*
[d]*Laboratory of Electronic Materials for Medical Application, Faculty of Sciences and Technology, University of Constantine 1, Constantine, Algeria*

Gas detection is vital for safety in important industrial and private sectors. Its major significance lies in its proactive risk mitigation, safeguarding lives and resources. In this paper, the focus is on the development of a gas sensor based on quartz crystal microbalance coated with a sensitive layer of zinc oxide (ZnO)–graphene nanocomposite for the detection of volatile organic compounds at room temperature. The incorporation of graphene or reduced graphene oxide is preferred in such applications due to their excellent electrical conductivity, chemical stability, and high surface area. These nanocomposites were synthesized using a chemical method via spray pyrolysis. Various techniques were employed to analyze the coated QCM electrode: contact angle measurements to assess surface wettability, Fourier transform infrared and energy-dispersive X-ray spectroscopy to investigate the composition of the coated electrode, and scanning electron and atomic force microscopies were used to study its surface morphology. These analyses provided valuable insights into the nanocomposite's interaction with the environment, composition, structure, and topography of the sensor's sensitive layer. To evaluate the sensor's sensitivity, the frequency shift ($\Delta f$) of the coated QCM electrode is monitored when exposed to different gas concentrations of ethanol, toluene, chloroform, humidity, and formamide, ranging from 47 to 142 ppm. The frequency shift indicated the detected gas concentration. The results demonstrate good repeatability and reversibility, which are crucial indicators of a sensor's reliability. This reliability is essential for applications in environmental monitoring or industrial safety, where accurate gas detection is critical.

topics: spray pyrolysis deposition, zinc oxide and graphene, gas sensor, quartz crystal microbalance (QCM)

## 1. Introduction

Gas sensing devices have an important role in many areas, from healthcare to industrial and environmental monitoring [1–5]. A quartz crystal microbalance (QCM) has been widely used as a highly sensitive device that can detect small changes in mass at room temperature, making it an excellent platform for gas-sensing applications [6]. The key to developing a QCM sensor is the choice of sensitive coating materials that interact with specific analytes effectively [7, 8].

Over the last decades, semiconductors have been considered very attractive sensitive coating materials, especially metal oxides, showing promise in chemical sensors. These materials offer advantages like low cost, easy production, and simple electronic measurement [9–12]. Among them, ZnO stands out as a well-known metal oxide capable of operating at room temperature. For these purposes, researchers have introduced different carbonaceous materials in the sensing matrices based on ZnO to improve electron migration and transportation which is the main element for sensing. Among

these materials, graphene or reduced graphene oxide (rGO) is one of the most promising components for chemical sensing at low operating temperatures [13–15]. According to the literature [16–18], graphene is composed of a unique 2D honeycomb lattice of $sp^2$-C atoms, the surfaces of which are decorated with several oxygenated functional groups and defect sites, which can provide enhanced sensing capability. When combined with metal oxide, a formation of p–n junctions between these two (metal oxides and graphene) induced a large specific surface area and a large number of defects and functional groups of graphene, which will facilitate molecular adsorption, gas diffusion, and mass transport, and improves the gas sensing properties. The research aimed to develop a gas sensor using an inexpensive quartz crystal microbalance (QCM) with a nanocomposite of zinc oxide (ZnO) and graphene as the sensing platform and sensitive layer, respectively. The ZnO–graphene nanocomposite was created through a chemical method, providing precise control over its composition and structure. A thin film of the nanocomposite was then applied to the QCM surface using the spray pyrolysis technique. The sensor's sensitivity was assessed by monitoring the frequency shift ($\Delta f$) of the coated QCM electrode at different concentrations of gases such as ethanol, toluene, chloroform, formamide, and water vapor. This frequency shift served as an indicator of the detected gas concentration, enabling quantitative analysis. Various analytical techniques, including contact angle measurements (CA), Fourier transform infrared spectroscopy (FTIR), scanning electron microscopy (SEM), energy-dispersive X-ray spectroscopy (EDAX), and atomic force microscopy (AFM), were used to analyze different aspects of the sensitive layer.

## 2. Materials and methods

### 2.1. Quartz crystal microbalance coating

In the QCM process, a sensitive layer composed of ZnO–graphene nanocomposites was created by using the spray pyrolysis technique. To achieve this, the substrates were placed on a hot plate, which was meticulously maintained at a temperature of 350°C with an accuracy of ±2°C. Zinc acetate dehydrate ($C_4H_6O_4Zn$) with an exceptional purity level of 99.99% was selected as the precursor salt for our initial solution, and 0.4 M of this solution was prepared by dissolving it in 50 mL of methanol. Subsequently, 0.1 g of home-made graphene powder was dispersed in 50 mL of ZnO solution. Graphene has been synthesized by following the Hummers method modified by recycling graphite rods from electrical storage devices [19, 20]. The suspension underwent room-temperature ultrasonication for one hour, resulting in a homogeneous solution of ZnO–graphene nanocomposites. This solution was subsequently loaded into a spray gun strategically positioned 20 cm above the substrate. Utilizing compressed air as the carrier gas, a fine mist of the precursor solution was generated. The spraying procedure was programmed as follows: 5 s spray time, followed by a 1 s break, repeated for a total of 60 cycles.

### 2.2. ZnO–graphene film characterization

Contact angle measurements were conducted at room temperature and atmospheric pressure to evaluate the wettability of the coated QCM surface. A 5 $\mu$L water droplet was carefully deposited onto the surface of the coated QCM using
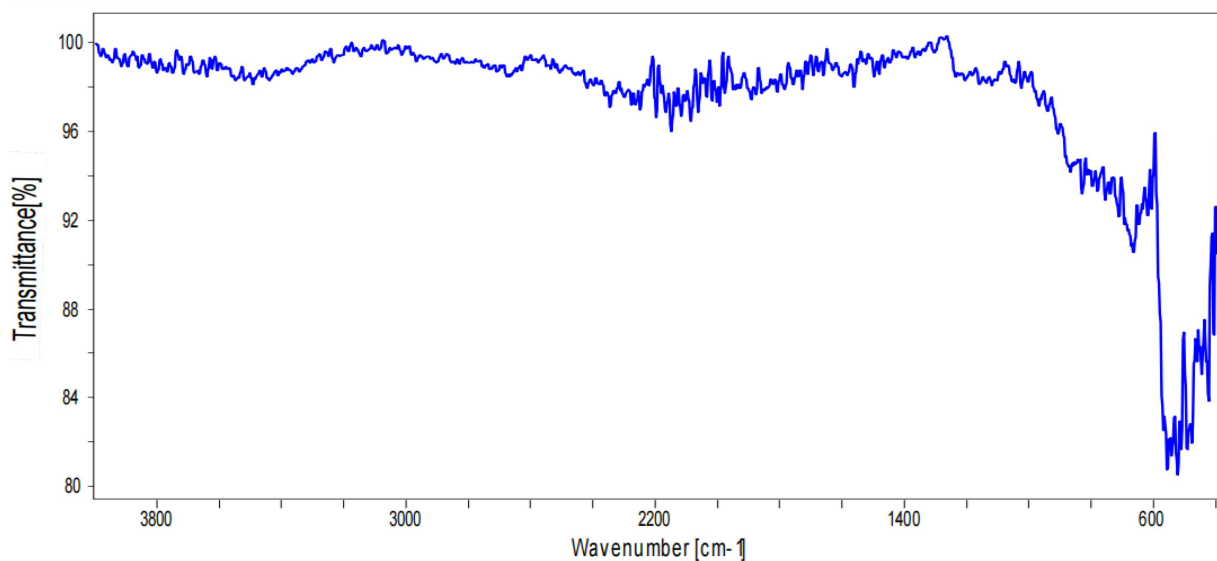


Fig. 1. FTIR spectra of ZnO–graphene nanocomposite sensitive layers.

a micro-syringe. Five measurements were performed, and the contact angle data were averaged, with a standard deviation of approximately 5%, to ensure reliable results.

FTIR spectroscopy was employed to analyze the chemical composition of each QCM coating. Spectra were recorded using a Thermo Nicolet Avatar 360 FTIR spectrometer. To investigate the surface morphology of the QCM coating, a scanning electron microscope (SEM) (ZEISS EVO MA 25) fitted with two Bruker XFlash $6-60$ X-ray detectors for energy-dispersive X-ray spectroscopy (EDAX) analysis and an atomic force microscope (AA2000, Angstrom Advanced Inc.) were utilized.

The principle of the QCM sensors is based on the change in the fundamental oscillation frequency ($\Delta f$) upon ad/absorption of molecules from the gas phase according to the Sauerbrey equation (Sauerbrey and Angew 1959 [21]). The piezoelectric crystals used were AT-cut 6 MHz quartz crystals. The frequency shifts of the vibrating crystal were directly monitored using LabVIEW software and a transistor Colpitts oscillator connected to the frequency counter TF930, TTi, as an interface controller. A liquid of known volume and density was introduced in a specific generating gas cell using a Hamilton syringe and then heated to evaporate freely. After evaporation, the vapor was injected into the sensitivity evaluation system.

The coated QCM-based sensor was evaluated for sensitivity by monitoring the frequency shifts of the quartz for different concentrations of volatile organic compounds vapors (VOCs vapors). The concentration of the introduced analyte was calculated in parts per million (ppm) [22]. After diffusion towards the electrode surface, the injected vapor was subsequently ad/absorbed by the functionalized QCM electrode, which displays a frequency shift ($\Delta f$). After the ad/absorption process was finished, the test chamber was purged with dry air until the end of the vapor desorption process. The sensor sensitivity was evaluated against concentrations of VOCs vapors. Inside the chamber, the humidity and temperature variations were monitored by a THT22 temperature and humidity sensor with an Arduino microcontroller.

## 3. Results and discussion

### 3.1. Sensitive layer surface characterization

FTIR spectroscopy was performed for the deposited ZnO–graphene to identify the vibrational modes. The spectrum was recorded in the frequency range of 400–4000 cm$^{-1}$. FTIR spectra of the sensitive layer are shown in Fig. 1.

A broad and strong peak at 3600–3300 cm$^{-1}$ is attributed to the O–H stretching vibration of the hydroxyl group, whereas the broadband observed around 2084–2350 cm$^{-1}$ indicates vibrations

related to the C–O bond. Smaller peaks in the 500–1000 cm$^{-1}$ range correspond to symmetric and asymmetric vibrations of C–O bonds, confirming the presence of carbon-containing material residues within the ZnO composite. The bands located around 2295 and 1600 cm$^{-1}$ are attributed to the stretching and bending modes of -OH groups, possibly originating from the adsorption of moisture when the sample was exposed to the atmosphere. Peaks at 1726, 1217, and 1055 cm$^{-1}$ are associated with the stretching and bending groups of C=O bonds, respectively [23]. These peaks align with existing research and indicate the specific chemical composition of the composite. Peaks at 1375 and 1222 cm$^{-1}$ are observed and correspond to bending vibration and stretching of hydroxyl groups (C–OH) edge. In the infrared region (400 to 800 cm$^{-1}$), peaks indicate stretching modes of Zn–O bonds, corresponding to hexagonal ZnO's vibrational mode. The absorbance peaks at about 1561 and 450 cm$^{-1}$ suggest the skeletal vibration of graphene sheets and the stretching vibration of Zn–O bonds, further supporting the concept of a composite structure involving both ZnO and graphene [24–26]. FTIR results correlate with what has been reported by M. Maruthupandy et al. [8] and E. Albiter et al. [27]. Overall, these FTIR results strongly suggest the successful formation of a composite structure integrating ZnO and graphene. The water contact angle measured on the QCM electrode surface coated with ZnO–graphene nanocomposite was found in the order of 30°, indicating the hydrophilic behavior of the QCM sensor surface with a good affinity toward polar molecules [28].

To further understand the morphology of these nanostructures, scanning electron and atomic force microscopies were performed, and the corresponding images are shown below in Figs. 2 and 3, respectively. SEM images (see Fig. 2a and 2b) clearly show that the surface of the nanocomposite thin film is adorned or decorated with two distinct types of nanoparticles, i.e., graphene nanoflakes and ZnO nanorods. Low-layer graphene nanoflakes were observed on the surface. These flakes have an average size of 200 nm. Graphene nanoflakes are thin, two-dimensional sheets of irregularly shaped graphene. These nanoflakes vary in size and shape, and their presence indicates the incorporation of graphene sheets or particles into the composite. ZnO nanorods were also present on the substrate. These nanorods range in particle size from 30 to 60 nm. Nanorods are 1D among ZnO nanostructures; they are used due to their large surface-to-volume ratio, low electron breakdown rate, and diverse surface topography, which are desirable for their detection performance, explaining the high sensitivity of our sensor. All these results were also reported by Y. Kang et al. [29] and M. Drobek et al. [30]. Moreover, these images and descriptions suggest that the ZnO–graphene nanocomposite
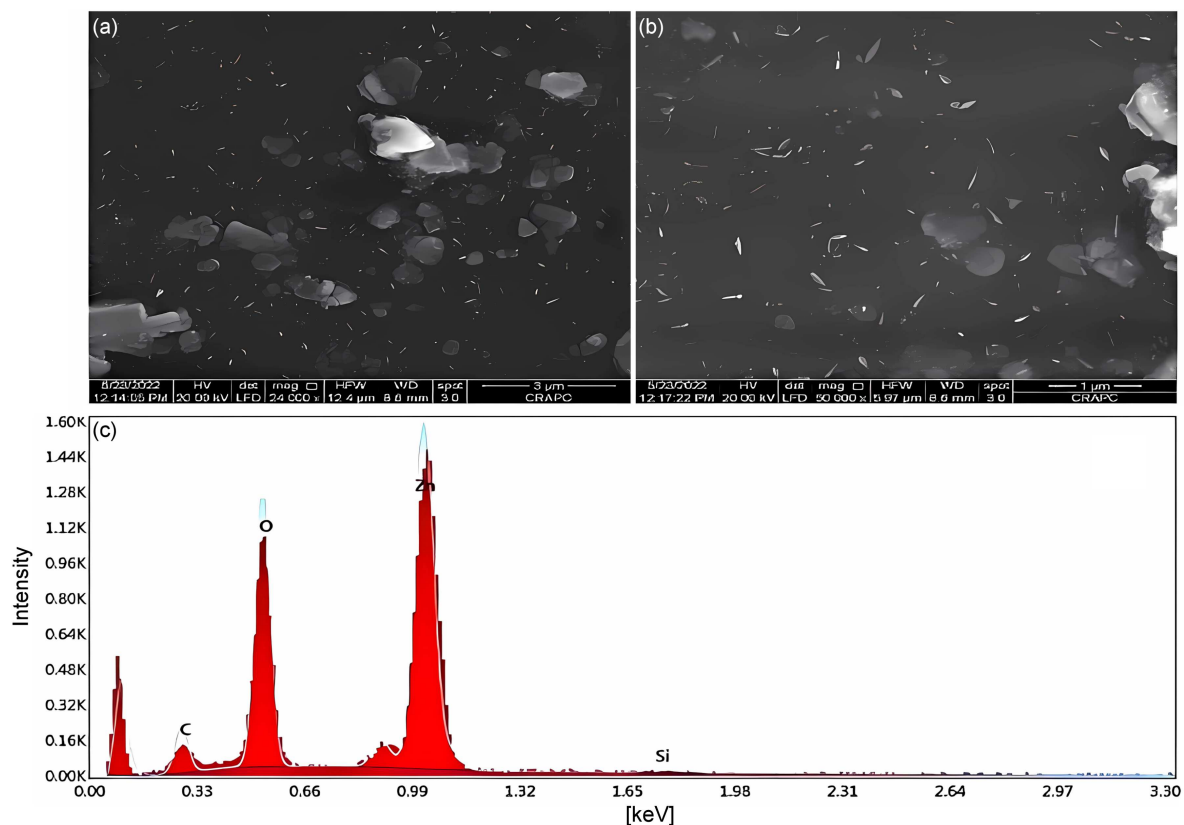
Fig. 2.   SEM images of ZnO–graphene nanocomposite sensitive layer (a) 3 $\mu$m, (b) 1 $\mu$m, and (c) EDAX pattern.
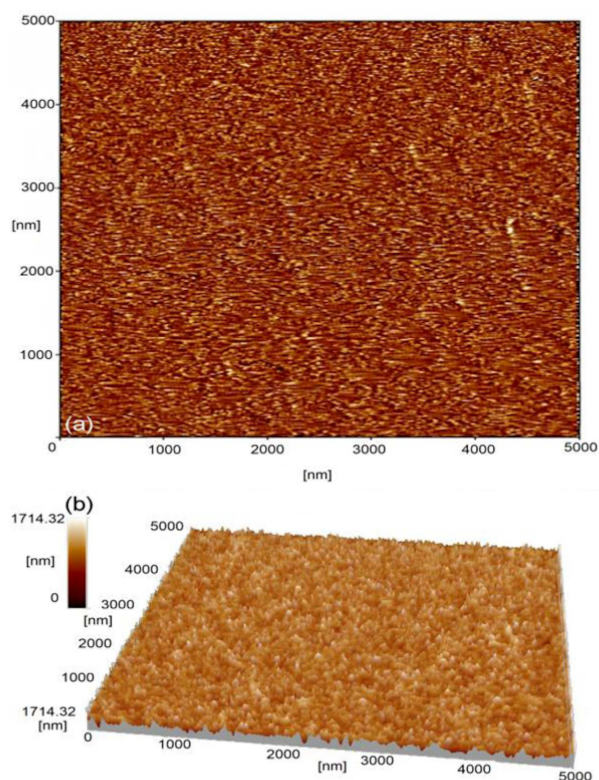


Fig. 3.   AFM images of ZnO–graphene nanocomposite sensitive layer (a) 2D and (b) 3D.

has been successfully deposited on silicon substrates, forming a structure with decorated surfaces consisting of graphene nanoparticles and ZnO nanorods. The presence of both materials and the observed distribution patterns are important for understanding the physical characteristics and potential applications of the nanocomposite. The formation of aggregates or agglomerates could be a result of interactions between the graphene nanoparticles and ZnO components during the deposition process. This information is crucial for optimizing the fabrication process and tailoring the properties of the composite for specific applications. The SEM images are similar to those found by Hasanzadeh Banakar et al. [31].

The elemental analysis of the deposited ZnO–graphene nanocomposite thin film has been accomplished by using EDAX analysis, as shown in Fig. 2c, confirming that no contaminants are deposited and only carbon, zinc, and oxygen are present in the deposited film on a silicon substrate, and the obtained element mapping confirms that. These results are in good agreement with the previous studies [24, 32]. Figure 3 depicts an AFM image ($5 \times 5$ $\mu$m$^2$) recorded on the QCM sensor surface coated with ZnO–graphene nanocomposite. The absence of pinholes indicates that the developed films have a homogeneous texture. The surface topography appears to exhibit a consistent
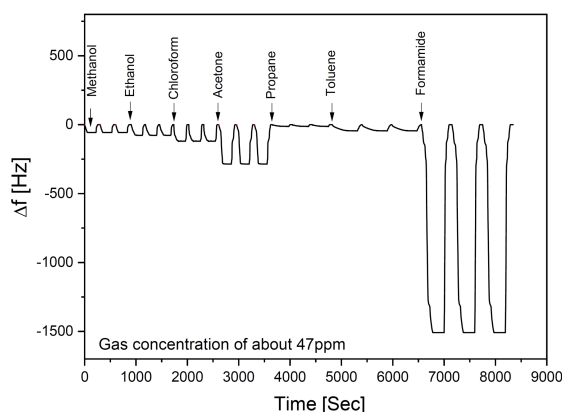
Fig. 4. The response/recovery to different gases of a QCM-based sensor coated with a thin layer of ZnO–graphene nanocomposite.

sea-island pattern[†1] [33]. Moreover, the root mean square roughness (RMS) value of this film was found to be 229 nm, which is an important value. The increase in surface roughness can be attributed to the presence of graphene particles and ZnO nanorods in the composite. The heightened roughness of the surface led to a larger specific surface area. This expanded surface area provides more sites for adsorption, explaining the enhanced adsorptive properties observed in the QCM sensor. In other words, the increased roughness allows the sensor to capture and detect more molecules, making it more effective.

### 3.2. Sensing performance

To evaluate the functionality of our sensor, the response was tested using two types of analytes: polar and non-polar molecules. This testing aimed to assess the sensor's response and its ability to detect and differentiate gases. The response/recovery of the QCM-based sensor coated with a thin layer of ZnO–graphene nanocomposite is shown in Fig. 4.

The response of the sensor is measured in frequency shift ($\Delta f$), which can be calculated by $\Delta f = f_{air} - f_{gas}$, where $f_{air}$ and $f_{gas}$ are the frequencies of QCM at air flow and gas flow conditions, respectively [32]. For all vapors, the isotherms showed that the absolute value of the shift frequency ($\Delta f$) increases gradually with time before reaching a constant value at a steady state. Between measurements, the sensor was exposed to dry air until full desorption was achieved. The frequency of the crystal returning to its initial state indicates

---

[†1]The sea-island pattern refers to a specific type of morphology or structure. It describes a formation where small "islands" of one material are dispersed within a continuous matrix of another material, resembling islands in a sea. This pattern is often created intentionally or unintentionally during the elaboration processing of composite materials.

full desorption of analytes from the coated electrode surface, proving reversibility. In addition, the kinetic response characteristics showed that the absolute value of $\Delta f$ increases progressively with time, then attaining a stable value. The sorption process achieves equilibrium when the adsorption and desorption processes have been occurring simultaneously [34]. To ensure repeatability, the experiments were repeated three times, and the relative standard deviation (RSD) was calculated.

Based on the above results, other tests have been performed to evaluate the response of our sensor toward different concentrations of VOCs vapors, as shown in Fig. 5a. It is seen that the sensors present a good affinity toward polar molecules compared to the non-polar ones. The responses are in the following ascending order: propane < toluene < methanol < ethanol < chloroform < acetone < formamide. For example, at a concentration of 90 ppm, acetone and formamide induce $\Delta f$ of −609 Hz and −2091 Hz, respectively; however, for the same concentration of propane and toluene, $\Delta f$ is −25 Hz and −82 Hz, respectively.

To evaluate the interaction between our sensor and water vapor, frequency responses at different vapor concentration levels were measured and compared to those at different formamide concentration levels. As shown in Fig. 5b, the ZnO–graphene nanocomposites-based sensor exhibits significantly higher sensitivity to formamide than to humidity (around 10 times higher), confirming that the sensor remains practically unaffected by water vapors.

Figure 6a and 6b depicts calibration response curves plotted against the maximum sensitivity observed on a QCM-based sensor coated with a thin layer of ZnO–graphene nanocomposite for humidity and VOCs vapors, respectively. All QCM sensor responses display linear relationships with changing analyte levels, showing an increase in frequency response as the levels increase. For instance, when exposed to formamide vapors at concentrations of 47, 89, and 142 ppm, the sensor registered responses of 1508, 2091, and 2500 Hz, respectively. These results confirm that the elaborated sensor is more sensitive to formamide and acetone.

Finally, the quantification was conducted using the standard addition method, and calibration curves were generated through linear regression. The obtained linearity was excellent, falling within the typical range of correlation coefficients ($R^2$) of 0.932 to 0.990. Achieving a correlation coefficient of at least 0.93 indicates a generally satisfactory characterization of the curve. The sensitivity, a critical parameter for a QCM sensor (the ratio of frequency change ($\Delta f$) to analyte vapor concentration change ($\Delta C$)), relative standard deviation (RSD), the sensor's response times for adsorption, desorption recovery for various molecules, limit of detection (LOD) (signal-to-noise ratio of 3), and the limit of quantitation (LOQ) (signal-to-noise ratio of 10) were calculated and summarized in Table I.

TABLE I

Characteristics performances of the elaborated sensors to the studied VOCs vapors.

| Gases | Sensitivity [Hz/ppm] | RSD [%] | LOD [ppm] | LOQ [ppm] | Responses times [s] | Recovery times [s] |
|---|---|---|---|---|---|---|
| methanol | 0.45 | 1.91–2.88 | 6.66 | 22.22 | 39 | 23 |
| ethanol | 1.288 | 1–2.45 | 2.34 | 7.76 | 58 | 33 |
| propane | 0.4 | 3.10–6 | 7.5 | 25 | 110 | 17 |
| chloroform | 1.89 | 1–4.25 | 1.58 | 7.81 | 47 | 19 |
| acetone | 6.46 | 2.81–3.66 | 0.46 | 1.55 | 26 | 32 |
| formamide | 10.44 | 1.42–3.92 | 0.29 | 0.96 | 87 | 27 |
| toluene | 0.43 | 3.10–5.86 | 6.97 | 23.25 | 128 | 58 |
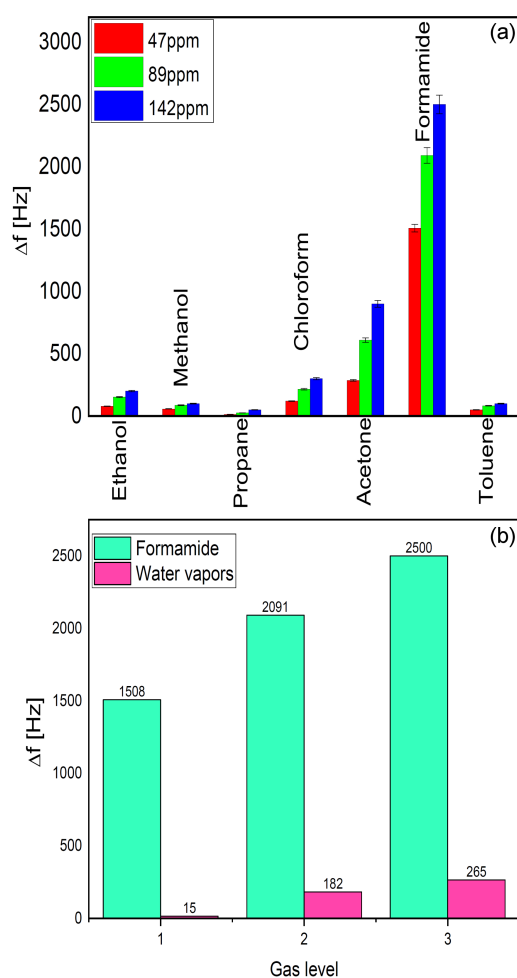


Fig. 5. Sensor's response to different concentrations of (a) VOCs vapors and (b) formamide compared to water vapor.



Fig. 6. Maximum sensitivity calibration curves of a QCM-based sensor coated with a thin layer of ZnO–graphene nanocomposite vs (a) water vapor, and (b) gas concentration.

In Table I, it is seen that formamide ($HCONH_2$) and acetone ($C_3H_6O$) exhibit the highest slope ratio among the various VOCs vapors, suggesting greater sensitivity. In addition, the mean values of RSD were in the range of 2 to 6%, which indicates that the QCM sensor responds in a reproducible manner for all types of gases. The response and recovery times are 26–87 s and 19–33 s, respectively, for polar molecules and 110–128 s and 17–58 s, respectively, for non-polar molecules. Using the determined LOD values, the developed sensor successfully identified little parts per million (ppm) of polar molecules.

By combining characterization results and detection performance, it can be assumed that the mass of the analyte depends on the number of graphene nanoflakes, ZnO nanorods, and agglomeration that

spread over the QCM electrode, with an increase in this number leading to an increase in roughness, hence improving gas detection properties. The principle of gas detection depends on the change in mass of the analyte on the coated QCM electrode. Analytes that are polar molecules cause van der Walls interaction with the hydrogen bond and COOH group of the engineered ZnO–graphene nanocomposite, resulting in a change in analyte mass on the QCM electrode surface. As a result, high-frequency shift variations are obtained, explaining the good affinity toward formamide and acetone vapors. The results are consistent with the study by Monika Gupta et al. [35] in "Graphene derivative coated QCM-based gas sensor for volatile organic compound (VOC) detection at room temperature" and with the work of Jie Li et al. [14] regarding the detection of n-propanol, which are polar molecules.

## 4. Conclusions

This paper describes the development of a new gas sensor using a ZnO-graphene nanocomposite thin film coated on a low-cost commercial quartz crystal microbalance. The sensor was fabricated using a spray pyrolysis method at 350°C, and it exhibited high sensitivity to polar molecules such as formamide and acetone at room temperature. The study also included an analysis of the reproducibility and sensitivity of the sensor for different vapor levels, as well as of the chemical, structural, and morphological properties of the sensitive film. The results indicated the successful formation of a composite structure incorporating ZnO and graphene, with the presence of -OH hydroxyl groups indicating the hydrophilic behavior of the sensitive film. Additionally, SEM images and EDAX analysis confirmed the presence of ZnO–graphene nanocomposite thin film, and AFM images revealed an increase in surface roughness, leading to a larger specific surface area for accommodating more active sites for VOCs molecule adsorption. Overall, the ZnO–graphene nanocomposite-based QCM sensor demonstrated high sensitivity towards the tested gases, making it suitable for environmental and industrial monitoring applications.

## Acknowledgments

## References

[1] M. Yıldırım, Ö.S. Bölukbaşı, Z.P. Özer, İ. Polat, N. Atar, M.L. Yola, *Ind. Eng. Chem. Res.* **62**, 4587 (2023).

[2] H.A. Deveci, M.M. Kaya, I. Kaya, B.B. Yola, N. Atar, M.L. Yola, *Biosensors* **13**, 725 (2023).

[3] G.F. Fine, L.M. Cavanagh, A. Afonja, R. Binions, *Sensors* **10**, 5469 (2010).

[4] T. Blank, L. Eksperiandova, K. Belikov, *Sens. Actuators B Chem.* **228**, 416 (2016).

[5] B.B. Yola, S. Bekerecioğlu, İ Polat, N. Atar, M.L. Yola, *Analyst* **148**, 3827 (2023).

[6] Y. Bakha, H. Khales, *Acta Phys. Pol. A* **136**, 490 (2019).

[7] V. Venkidusamy, S. Nallusamy, G. Nammalvar, R. Veerabahu, A. Thirumurugan, C. Natarajan, S.S. Dhanabalan, D.P. Pabba, C.V. Abarzúa, S.-K. Kamaraj, *Micromachines* **14**, 189 (2023).

[8] M. Maruthupandy, P. Qin, T. Muneeswaran, G. Rajivgandhi, F. Quero, J.-M. Song, *Mater. Sci. Eng. B* **254**, 114516 (2020).

[9] A. Ma, H.J. Park, J.H. Seo, K.Y. Jang, H.K. Lee, J.E. Lee, K.M. Nam, D.-S. Lee, *Sens. Actuators B Chem.* **308**, 127698 (2020).

[10] W. Qin, Z. Yuan, H. Gao, R. Zhang, F. Meng, *Sens. Actuators B Chem.* **341**, 130015 (2021).

[11] H. Ji, W. Qin, Z. Yuan, F. Meng, *Sens. Actuators B Chem.* **348**, 130698 (2021).

[12] Y. Bakha, S.M. Merah, H. Khales, M. Kameche, A. Djelloul, *Appl. Phys. A* **129**, 363 (2023).

[13] W. Feng, Y. Wang, J. Chen, L. Wang, L. Guo, J. Ouyang, D. Jia, Y. Zhou, *Carbon* **108**, 52 (2016).

[14] J. Li, Z. Jin, Y. Chao, A. Wang, D. Wang, S. Chen, Q. Qian, *Chemosensors* **11**, 65 (2023).

[15] E. Salih, M. Mekawy, R.Y. Hassan, I.M. El-Sherbiny, *J. Nanostruct. Chem.* **6**, 137 (2016).

[16] S.B. Kang, A. Sanger, M.H. Jeong, J.M. Baik, K.J. Choi, *Sens. Actuators B Chem.* **379**, 133196 (2023).

[17] S. Sen, S. Kundu, *J. Alloys Compd.* **881**, 160406 (2021).

[18] J. Qiu, X. Hu, X. Min, W. Quan, R. Tian, P. Ji, H. Zheng, W. Qin, H. Wang, T. Pan, *ACS Appl. Mater. Interfaces* **12**, 19755 (2020).

[19] H. Bakli, M. Moualhi, M. Makhlouf, *Meas. Sci. Technol.* **33**, 045012 (2022).

[20] M. Kadari, M. Makhlouf, *Mater. Today Proc.* **49**, 1093 (2022).

[21] G. Sauerbrey, *Z. Phys.* **155**, 206 (1959).

[22] M. Boutamine, O. Lezzar, A. Bellel, K. Aguir, S. Sahli, P. Raynaud, *Anal. Lett.* **51**, 387 (2018).

[23] J. Wu, X. Shen, L. Jiang, K. Wang, K. Chen, *Appl. Surf. Sci.* **256**, 2826 (2010).

[24] M. Saranya, R. Ramachandran, F. Wang, *J. Sci. Adv. Mater. Devices* **1**, 454 (2016).

[25] R.A. Mahmud, A.N. Shafawi, K.A. Ali, L.K. Putri, N.I.M. Rosli, A.R. Mohamed, *Mater. Res. Bull.* **128**, 110876 (2020).

[26] K.M. Al Aqad, C. Basheer, *J. Physical Org. Chem.* **34**, e4117 (2021).

[27] E. Albiter, A.S. Merlano, E. Rojas, J.M. Barrera-Andrade, Á. Salazar, M.A. Valenzuela, *J. Compos. Sci.* **5**, 4 (2020).

[28] S. Nundy, A. Ghosh, T.K. Mallick, *ACS Omega* **5**, 1033 (2020).

[29] Y. Kang, F. Yu, L. Zhang, W. Wang, L. Chen, Y. Li, *Solid State Ion.* **360**, 115544 (2021).

[30] M. Drobek, J.-H. Kim, M. Bechelany, C. Vallicari, A. Julbe, S.S. Kim, *ACS Appl. Mater. Interfaces* **8**, 8323 (2016).

[31] S.H. Banakar, M.G. Dekamin, A. Yaghoubi, *New J. Chem.* **42**, 14246 (2018).

[32] S. Sharma, S. Vyas, C. Periasamy, P. Chakrabarti, *Superlattices Microstruct.* **75**, 378 (2014).

[33] A. Ivanov, N. Nebogatikova, I. Kotin, I. Antonova, *Phys. Chem. Chem. Phys.* **19**, 19010 (2017).

[34] M. Boutamine, A. Bellel, S. Sahli, Y. Segui, P. Raynaud, *Thin Solid Films* **552**, 196 (2014).

[35] M. Gupta, N. Athirah, H.F. Hawari, *Indones. J. Electr. Eng. Comput. Sci.* **18**, 1279 (2020).